Research Article | Vol. 32, No. 20 / 23 Sep 2024 / Optics Express 35202
Optics EXPRESS

Large power dynamic range microwave electric field sensing in a vapor cell

MEIYU MA,[1,2] SANDAN WANG,[1,2] YANG YAN,[1,2] JINPENG YUAN,[1,2,3] LINJIE ZHANG,[1,2] LIRONG WANG,[1,2,4] LIANTUAN XIAO,[1,2] AND SUOTANG JIA[1,2]

[1]State Key Laboratory of Quantum Optics and Quantum Optics Devices, Institute of Laser Spectroscopy, Shanxi University, 92 Wucheng Road, Taiyuan 030006, China
[2]Collaborative Innovation Center of Extreme Optics, Shanxi University, 92 Wucheng Road, Taiyuan 030006, China
[3]yjp@sxu.edu.cn
[4]wlr@sxu.edu.cn

Abstract: Sensing of the microwave (MW) electric field with high accuracy and large power dynamic range has assisted in the implementation of metrology and communication. Here, an atom−based MW sensing system with a large linear power dynamic range for an electric field in the C band of 6.835 GHz is demonstrated in a vapor cell. The Rydberg electromagnetically induced transparency (EIT) spectra involving $53D_{5/2}$ state are employed to measure the medium intensity electric field by AC stark effect. On this basis, the heterodyne method, adding an auxiliary local oscillator (LO) MW field as a gain, is employed to measure the weak electric field. Finally, the strong electric field sensing is achieved by the atomic Rabi resonance when the coupling laser is turned off. As a result, the MW electric field measurements with a large linear power dynamic range of 101.6 dB are reached in a vapor cell by using multi−cooperative measurement methods. This work provides an effective approach for realizing the quantum MW sensing with high sensitivity and large power dynamic range.

1. Introduction

The microwave (MW) electric field sensing is important for a wide range of applications in the areas of modern communications, remote sensing, location, fiber optic sensing, and military science [1–4]. The atomic ensemble, featuring of hyperfine energy level structure, holds tremendous promise for precision measurement of fundamental physical quantities such as time, length, gravitational acceleration, magnetic and electric fields [5–14]. As an emerging technology, the atom−based MW electromagnetic fields sensors have the advantages of high repeatability, high stability, and International System of Units (SI) traceability [9,15,16].

Rydberg atoms have the remarkable properties of large dipole moments, long radiative lifetime, and large polarizability [17]. The Rydberg atom−based sensors with the outstanding characteristics of high sensitivity and broad bandwidth have been seen growing interest for a range of applications in MW sensing, metrology, imaging, and communication [15,18–23]. Recently, the Rydberg atom−based sensors are widely used for MW electric field measurements, including the MW field strength [8,24,25], polarization [26], phase [27] and angle−of−arrival [28]. Meanwhile, the atom−based MW magnetic field sensing, taking advantage of Rabi resonances induced by a phase modulated resonant MW field [29,30], has shown broad application prospect in microwave magnetic field stabilization [9], microwave imaging [31], and materials characterization [32].

Maintaining linear response characteristics in the large power dynamic range is an ongoing goal of MW electric field sensing. The off-resonant AC Stark effect of Rydberg atoms is a common means of continuously tunable MW electric field sensing [33–35] for achieving electric field measurements of hundreds of millivolts per centimeter. However, the AC stark spectrum

#537843 https://doi.org/10.1364/OE.537843
Journal © 2024 Received 29 Jul 2024; revised 31 Aug 2024; accepted 31 Aug 2024; published 13 Sep 2024

Optics EXPRESS

shows indistinguishable stark shift and splitting with the weak electric field intensity due to the limitation of spectral linewidth. In order to achieve the weak electric field measurement limit, the rising heterodyne measurement method based on Rydberg atoms has emerged by converting the measurement of frequency splitting into the measurement of modulation amplitude [25,36–39]. On the other hand, when the electric field intensity is strong, the peak of the AC stark spectrum becomes unrecognizable due to the power broadening effect, complicating the measurement of strong MW electric field [40]. Fortunately, the Rabi resonance method provides a solution for measuring strong MW electric field intensity [41]. Moreover, the MW magnetic field sensing based on Rabi resonance offers frequency tunability in the presence of external static magnetic field [42]. However, the aforementioned independent measurement methods only offer means for realizing MW electric field measurement with varying intensities. Developing a unified approach by merging multiple measurement methods to achieve MW electric field sensing with a large linear dynamic range and wide operating bandwidth remains an ongoing goal.

In this work, an atom−based MW sensing with large linear dynamic power range is performed for electric field measurement of 6.835 GHz in an ^{87}Rb atomic system. The Rydberg electromagnetically induced transparency (EIT) spectra with $5S_{1/2} - 5P_{3/2} - 53D_{5/2}$ transition are used to read out the medium intensity electric field by AC stark effect. Furthermore, the heterodyne method is employed to measure the weak electric field by adding an auxiliary local oscillator (LO) MW field as a gain. Finally, the atomic Rabi resonance is utilized for strong MW electric field sensing when the coupling laser is turned off. As a result, the MW electric field measurements with a linear power dynamic range of 101.6 dB are achieved by the multiplexing system, which paves the way for the integration of electromagnetic field sensing for meeting more common practical application requirements.

2. Theoretical model

When the MW field with a frequency of 6.835 GHz interacting with atoms, the atomic response depends on the intensity of the MW field. The energy level of Rydberg atoms experiences stark shift and splitting when exposed to a moderate MW field. The square of electric field intensity E is proportional to the stark shift Δf_{stark}, which is described by [43]:

$$E = \sqrt{\frac{-2\Delta f_{stark}}{\alpha}} \tag{1}$$

where α is the atomic polarizability of the $53D_{5/2}(m_j = 5/2)$, which is calculated with 322.64 MHz cm^2 V^{-2} in a field range of $0 - 2$ V/cm by using Alkali Rydberg Calculator (ARC) [44]. The Δf is the measured frequency stark shift when scanning the coupling laser. However, due to the limitation of linewidth, the linear power dynamic range of electric field intensity measurement based on the Stark effect is relatively narrow.

When the MW field is weaker, the energy level shift and disturbance of the Rydberg atomic group is small, making it difficult to measure extremely weak electric field intensity by the small frequency stark shift [43]. The heterodyne method provides a solution for observing the atomic response to weak SIG electric field, which converts the frequency splitting measurement to the modulation amplitude measurement by adding a LO field. Taking the SIG field as $E_{SIG}cos(\omega_{SIG}t + \phi_{SIG})$ and the LO field as $E_{LO}cos(\omega_{LO}t + \phi_{LO})$, the intensity of SIG field is read out by the atomic response with the given presence of the LO field. When the LO field and the SIG field are incident on the atomic vapor cell, the total MW electric field (E_{tot}) in the Stark shift regime far from the atomic resonance can be expressed as [27]:

$$E_{tot}^2 = E_{LO}^2 + E_{SIG}^2 + 2E_{LO}E_{SIG}cos(\Delta\omega t + \Delta\phi) \tag{2}$$

where $E_{LO}(E_{SIG})$ represent the amplitude of the LO field (SIG field), $\Delta\omega = \omega_{LO} - \omega_{SIG}$ and $\Delta\phi = \phi_{LO} - \phi_{SIG}$ are the difference of the angular frequency and phase between the LO field and

Optics EXPRESS

the SIG field, respectively. For the situation of weak field ($E_{SIG} \ll E_{LO}$), the weak SIG electric field intensity is obtained by Eq. (2):

$$E_{tot} \approx E_{LO} + E_{SIG}\cos(\Delta\omega t + \Delta\phi) \tag{3}$$

The Rydberg−EIT signal oscillates with frequency difference $\delta = \Delta\omega$ between SIG and LO fields in the Stark shift, which is obtained spectroscopically by combining the Eqs. (1) and (3). Note that, the obtained oscillation signal intensity increases linearly with both the intensity of SIG and LO fields, meaning the response of the SIG field intensity for Rydberg atoms increases linearly with the addition LO field as a heterodyne gain.

Furthermore, as the MW field intensity increases, the spectral peaks of Rydberg−EIT almost disappear owing to the power broadening effect. Simultaneously, the phase−modulated MW field resonates with the atoms possessing Zeeman sublevels, thereby exciting the ground state magnetic dipole transition to generate a Rabi resonance signal. The amplitude of the Rabi resonance signal P_β is expressed as a function of the phase modulation frequency ω_m under the small signal approximation [31,45]:

$$P_\beta \propto \frac{\theta^2\omega_m\Omega^2}{\sqrt{(\Omega^2 - 4\omega_m^2)^2 + 4\gamma_1^2\omega_m^2}} \tag{4}$$

where θ is phase modulation index, Ω is Rabi frequency, γ_1 is the longitudinal relaxation rate. Obviously, the value of P_β reaches its maximum when the Rabi frequency is $\Omega = 2\omega_m$. Furthermore, the Ω is depend on the magnetic field intensity H according to quantum theory [31]:

$$\Omega = \frac{g_J\mu_0\mu_B\langle F, m_F|J|F+1, m_F\rangle}{\hbar}H \tag{5}$$

where $\hbar$ is the reduced Planck's constant, g_J is the Landé g−factor, μ_0 is the permeability, μ_B is the Bohr magneton, $\langle F, m_F|J|F+1, m_F\rangle$ represents the matrix element, and J is the component of the electron angular momentum. Therefore, the strong magnetic field intensity measurement with high accuracy can be achieved by the Rabi resonance method. According to Maxwell's equations, MW magnetic field measurement is equivalent to the measurement of the electric field at the same power level. In summary, the atom−based electric field sensing with large linear power dynamic range is attained by employing multiple cooperative measurement methods.

3. Experimental setup

The relevant atomic energy levels employed in this experiment are illustrated in Fig. 1(a). A probe field at 780 nm drives ^{87}Rb atoms from the ground state $5S_{1/2}(F = 2)$ to the intermediate state $5P_{3/2}(F' = 3)$, while a coupling field at 480 nm excites atoms from the intermediate state $5P_{3/2}(F' = 3)$ to the Rydberg state $53D_{5/2}$. The SIG MW field with the frequency of 6.835 GHz is used to excite the magnetic dipole transitions of ^{87}Rb $5S_{1/2}(F = 1) - 5S_{1/2}(F = 2)$ and cause the Rydberg state of $53D_{5/2}$ stark frequency shift and splitting for SIG magnetic and electric field measurements, respectively. A LO field with a frequency difference of 100 kHz from the SIG field is provided for achieving heterodyne measurement of the SIG electric field.

Figure 1(b) shows the sketch of the experimental setup for large power dynamic range MW electric field sensing. A probe laser of 780 nm drives ^{87}Rb atoms from the ground state $5S_{1/2}(F = 2)$ to the $5P_{3/2}(F' = 3)$ state, which is provided by an external cavity diode laser (DL pro, Toptica). The coupling laser of 480 nm continually excites atoms $5P_{3/2}(F' = 3)-53D_{5/2}$ transition by a frequency−doubled amplified diode laser (DLC TA−SHG pro, Toptica). Meanwhile, the 780 nm and 480 nm lasers are locked by saturation absorption spectrum and EIT spectrum for their frequency references, respectively. The ^{87}Rb atoms in the experiment are filled into a

Optics EXPRESS

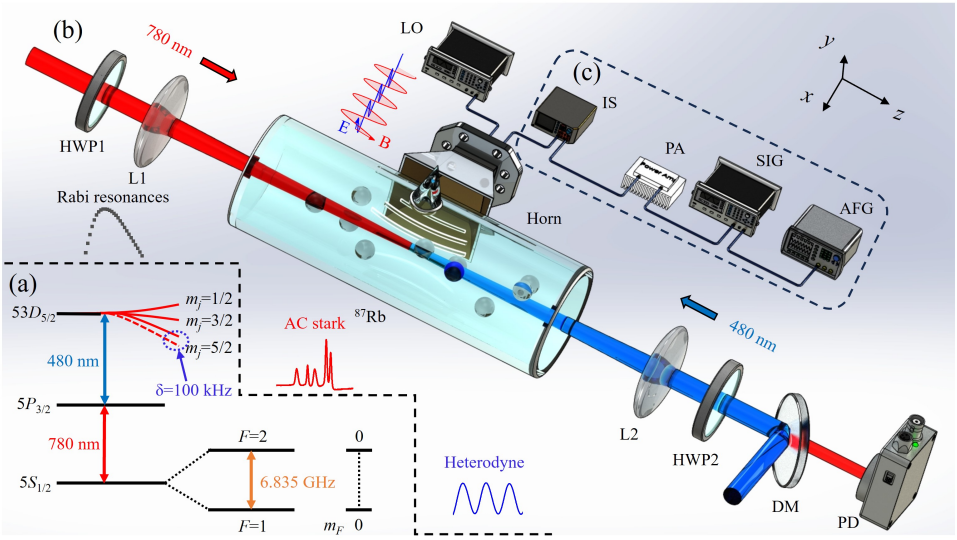

Fig. 1. (a) The relevant energy levels diagram of ^{87}Rb atoms. (b) The schematic of the experimental setup. HWP, half−wave plate; L, lens; DM, dichroic mirror; PD, photodiode detector; LO, local oscillator vector signal generator; IS, isolators; PA, power amplifier; SIG, signal vector signal generator; AFG, arbitrary function generator. (c) Electromagnetic signal generation device. The red, blue, and black spectral signal represent the initial signals of AC stark, heterodyne, and Rabi resonance, respectively.

cylindrical room−temperature vapor cell with 75 mm long and 25 mm in diameter. The probe laser beam overlaps with coupling laser beam in the Rb vapor cell by a counter−propagation configuration. The power of probe and coupling beams are 100 μW and 120 mW with beam diameters of 100 μm and 150 μm in the rubidium vapor cell, corresponding the Rabi frequencies of $33.6 \times 2\pi$ and $18 \times 2\pi$ MHz, respectively.

The electromagnetic signal generation device, comprising vector signal generator (SIG), isolators (IS), power amplifier (PA), and arbitrary function generator (AFG), is depicted by the Fig. 1(c). The SIG MW field with frequency of 6.835 GHz is generated by vector signal generators (SMB100A, Rohde & Schwarz). A power amplifier (PA) is loaded for power amplification and isolated by an isolator (IS) for protecting the devices. The horn is used to radiate MW electromagnetic fields. Two half wave plates (HWP1 and HWP2) are used to adjust polarization direction of the laser beams for keeping the polarization consistency among the laser and the MW fields. A photodiode detector (PD) is utilized to detect the probe beam carrying MW field information. The obtained spectral signals are recorded and analyzed by the oscilloscope (RTO2004 oscilloscope, Rohde & Schwarz) and spectrum analyzer (EXA signal analyzer, Keysight), respectively.

The Rydberg−EIT spectra are obtained by locking probe laser and scanning coupling laser frequency for medium intensity MW electric field measurement with AC Stark effect. On this basis, a LO MW field (SMB100A, Rohde & Schwarz) with 0.27 V/cm intensity is introduced to complete weak MW electric field measurement based on heterodyne method. Furthermore, when turning off the coupling laser, the strong MW magnetic field is measured by the Rabi resonance signal, which is obtained by phase modulation of SIG MW field (0 − 14 kHz) using an arbitrary function signal generator (AFG) (Tektronix AFG 3022C).

Optics EXPRESS

4. Experimental results and discussions

The Rydberg−EIT spectra of $53D_{5/2}$ state with different SIG field intensity E are shown in Fig. 2(a), which is used to demonstrate the AC Stark spectra at a MW frequency of 6.835 GHz. The field−free EIT spectrum with E = 0 V/cm is obtained by scanning the detuning of the coupling laser Δ_c, as shown in top red curve. Furthermore, the EIT spectra is measured when the SIG field intensity is E = 0.17, 0.55 and 2.1 V/cm, which are displayed by green, orange, and purple curves, respectively. The stark shifts and splitting of EIT spectra are observed due to the degeneracy of the magnetic substates with m_j = 1/2, 3/2, 5/2 becomes lifted in the presence of SIG field.

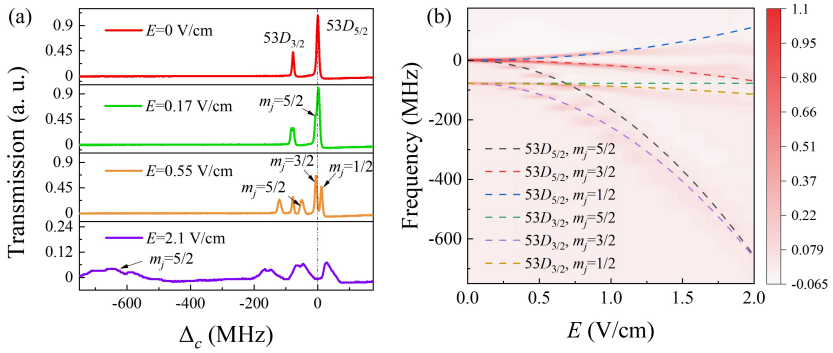

Fig. 2. (a) The measured Rydberg−EIT spectra for the $53D_{5/2}$ state with SIG field of E = 0 (red curve), 0.17 (green curve), 0.55 (orange curve), and 2.1 V/cm (purple curve), respectively. (b) The AC Stark spectra of the Rydberg states $53D_{5/2}$ and $53D_{3/2}$ by varying the SIG field in a range of 0 − 2 V/cm. The colored dashed lines are the calculated Stark shift of $53D_{5/2}$ and $53D_{3/2}$ states.

Figure 2(b) demonstrate the contour plots of a series of Rydberg−EIT spectra by varying the SIG field from 0 to 2 V/cm with a step of 0.17 V/cm. The Stark shifts and splitting of Rydberg−EIT with $53D_{5/2}$ (m_j = 1/2, 3/2, 5/2) states occur simultaneously when increasing SIG field intensity. Comparing with the $53D_{5/2}$ (m_j = 3/2, 1/2) states, the Rydberg−EIT spectrum of $53D_{5/2}$ (m_j = 5/2) state represents the larger Stark shift owing to the larger polarizability, which is more sensitive to the electric field measurement. Therefore, the $53D_{5/2}$ (m_j = 5/2) state is selected for the SIG field measurements by Eq. (1). The Stark shift of $53D_{5/2}$ and $53D_{3/2}$ states are calculated by using ARC, as shown in the colors dashed lines of Fig. 2(b). The experimental SIG electric field (x−axis) is calibrated by the theoretical calculations. However, the above AC Stark effect is only applicable for medium intensity electric field measurement due to limitation of Rydberg−EIT spectral linewidth. When the intensity of MW electric field is too small, the spectrum exhibits indistinguishable stark shifts as shown in the green curve in Fig. 2(a). Additionally, the Rydberg−EIT spectral peaks almost disappear in the areas of strong electric field owing to the power broadening effect, as shown in the purple curve of Fig. 2(a).

The weaker MW electric field measurement is achieved by heterodyne method when introducing the optimal LO field of E_{LO} = 0.27 V/cm. Figure 3(a) presents the measured probe laser transmission signals of LO and SIG fields with the SIG field power of −10 (orange line), 0 (green line), and 10 dBm (red line), respectively. The coupling laser is locked to the Rydberg−EIT spectra peak of $53D_{5/2}$ (m_j = 5/2) state. The probe laser transmission signals show periodic oscillation with a period of 100 kHz. Meanwhile, the amplitude of oscillation signals increases with the increasing SIG field intensity, which are measured by a spectrum analyzer with a resolution bandwidth of 2 Hz and a video bandwidth of 2 Hz. The relationship of oscillation

Optics EXPRESS

signals output amplitude and SIG field power are shown in Fig. 3(b). The dots are experimental measurement results while the orange, green and red dots correspond to the oscillation signals in Fig. 3(a), respectively. The red line represents the fitting curve. It can be found that the output amplitude of the oscillation signals linearly increases when the SIG field power is increased from −60 to 15 dBm.

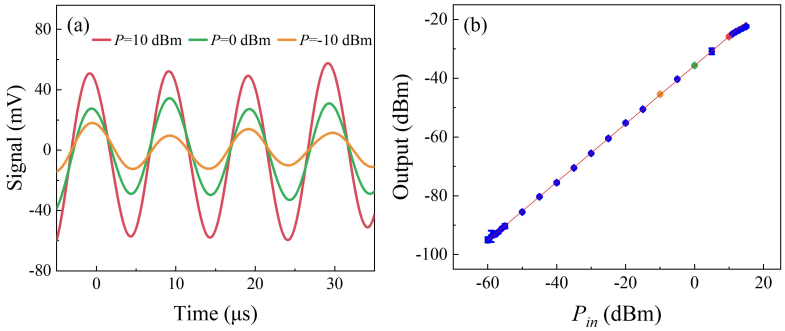

Fig. 3. (a) The probe laser transmission signals at the time domain with fixed LO field E_{LO} = 0.27 V/cm for the SIG MW power of −10, 0, and 10 dBm, respectively. (b) The measured amplitude of probe laser transmission signals with SIG field power in the weak field region by using a spectrum analyzer. The dots represent the experimental measurement results, where the colored dots correspond to the signal in (a). The red line is the fitting curve. The errors are the standard deviation of the three measurements.

The strong MW magnetic field is measured by the Rabi resonance method when the Zeeman transitions of ^{87}Rb atoms $5S_{1/2}(F = 1) - 5S_{1/2}(F = 2)$ is excited by a phase modulated SIG MW field in the presence of only a probe laser. Figure 4(a) depicts several Rabi resonances signals as the function of phase modulation frequency ω_m for different SIG field power of 35.6, 38.1, 40, and 40.8 dBm, respectively. The Rabi frequency Ω with 9.20, 10.47, 11.53, and 12.13 kHz of the MW magnetic field is obtained by fitting the experimental data under the equation of $\Omega = 2\omega_m$. Furthermore, the MW magnetic field intensity (B) is measured by the Ω according to Eq. (5). Figure 4(b) shows the obtained MW magnetic field intensity as a function of the square root of the MW power ($\sqrt{P}$). The data represent the experimental measurement results, and the red line is the fitting curve. It can be found that the B linearly increases with 0.66 − 0.91 μT when the SIG field power is increased from 35.6 to 41.6 dBm. According to the dependence relationship between MW electric and magnetic field, the measurement of MW magnetic field can be equivalent to the measurement of MW electric field at the same power level. It is worth noting, the microwave magnetic field and electric field are radiated by the same vector signal generator without changing the radiation source.

Figure 5 shows the results of electric field measurements with a large power linear dynamic range by using three different measurement methods. A modified radar equation of $E_{SIG} = a\frac{\sqrt{30P \cdot g}}{d}$ is used to deduce the calibrated electric field with different MW power at the vapor cell, where the E_{SIG} is the SIG electric field intensity, g is the gain factor of the antenna, d is the distance between the horn antenna port and the center of the rubidium cell, and a is the cell perturbation factor fitted by experimental results [16,46]. In our experiment, the g of the horn is 20 dB and the d between the antenna and the atoms remains 1 cm. Therefore, the modified radar equation can be simplified as $E_{SIG} = F\sqrt{P}$, where F represents the calibration transmission factor for electric field measurement obtained by $E_{stark} = F\sqrt{P}$ in a moderately strong field region, the E_{stark} is obtained MW electric intensity by the AC Stark spectrum for the $53D_{5/2}$ (m_j = 5/2) state using Eq. (1).

Optics EXPRESS

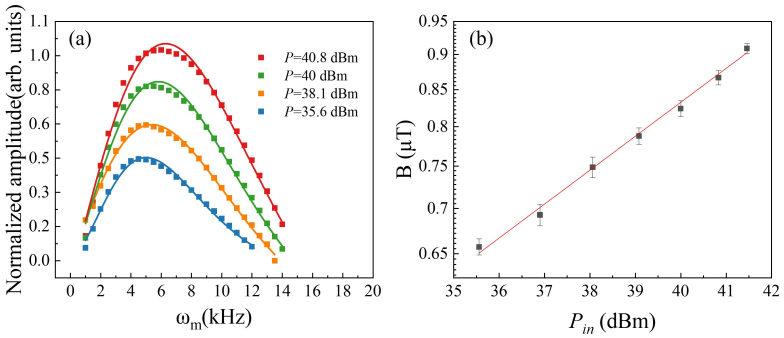

Fig. 4. (a) The Rabi resonance signal with a SIG field frequency of 6.835 GHz and power of 35.6, 38.1, 40 and 40.8 dBm, respectively. (b) The measured peak value of the Rabi resonance signal corresponding to the different SIG field power in the strong field region by using a spectrum analyzer. The data represent the experimental measurement results, and the line is the fitting curve. The errors are the standard deviation of the three measurements.

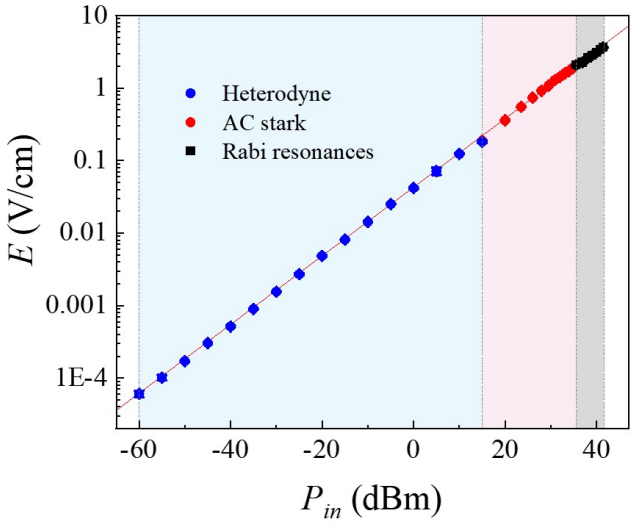

Fig. 5. The MW electric field intensities as a function of SIG field power based on heterodyne (blue dots), AC stark effect (red dots), and Rabi resonance (black squares) in the large power linear dynamic range. The data represent the experimental measurement results, and the line is the fitting curve. The blue, pink, and gray regions correspond to the linear regions of SIG field power and field intensity for above three measurement methods, respectively. The errors are the standard deviation of the three measurements.

The relationship between the E_{stark} and MW power is shown in the red dots of Fig. 5. The average value of F = 0.03422 V cm^{-1} mW$^{-1/2}$ is calibrated by linear fitting of twelve sets of data from different MW fields. Furthermore, the applied SIG field intensity in the weak regions is acquired by calibrated F with heterodyne method, as shown in the blue dots of Fig. 5. Similarly, the relationship between MW magnetic field intensity and MW field power is written as $B_{SIG} = K\sqrt{P}$, where K is calibrated transmission factor for the measured magnetic field by Rabi resonance $B_{Rabi} = K\sqrt{P}$, and K = 0.0042 μT mW$^{-1/2}$ in the strong field region obtained by linear fitting of Fig. 4(b). According to the Maxwell equations [47], a linear transformation relationship between MW electric field and magnetic field components can be established as

Optics EXPRESS

$E_{SIG} = \frac{F}{K} B_{SIG}$ [41]. Therefore, the equivalent electric field is measured by Rabi resonance, which is depicted by the black square of Fig. 5. To sum up, the MW electric field measurement with a linear power dynamic range of 101.6 dB is achieved by the multi−cooperative measurement methods in Rb vapor cell. Moreover, the multi-cooperative measurement method can be extended to other working frequencies [35,42].

5. Conclusions

In summary, we demonstrated a large power dynamic range MW electric field sensing of 6.835 GHz in a Rb vapor cell. The Rydberg−EIT spectra involving $53D_{5/2}$ state are used to read out the medium intensity electric field by AC Stark effect with power dynamic range of 20.6 dB. The heterodyne method is applied to measure the weak electric field with power dynamic range of 75 dB by adding an auxiliary LO MW field as a gain. Meanwhile, the strong electric field sensing with power dynamic range of 6 dB is achieved based on the atomic Rabi resonance while the coupling laser is turned off. Finally, the electric field sensing with a linear dynamic power range of 101.6 dB is realized in a Rb vapor cell. This work has the potential for improving the practical application value of quantum microwave sensing and communication.

Funding. Innovation Program for Quantum Science and Technology (2023ZD0300902); National Natural Science Foundation of China (12474359, 62075121, 62475136); Fundamental Research Program of Shanxi Province (202403021211158); Fund Program for the Scientific Activities of Selected Returned Overseas Professionals in Shanxi Province (2023001); Shanxi Scholarship Council of China (2024-003); the Fund for Postdoctoral Fellowship Program of China Postdoctoral Science Foundation (GZC20231510); the Fund for Shanxi 1331 Project.

Disclosures. The authors declare no conflicts of interest.

Data availability. Data underlying the results presented in this paper are not publicly available at this time but may be obtained from the authors upon reasonable request.

References

1. K. C. Cox, D. H. Meyer, F. K. Fatemi, *et al.*, "Quantum-limited atomic receiver in the electrically small regime," Phys. Rev. Lett. **121**(11), 110502 (2018).
2. P. H. Swain and S. M. Davis, "Remote sensing: The quantitative approach," IEEE Trans. Pattern Anal. Mach. Intell. **PAMI-3**(6), 713–714 (1981).
3. Y. Yan, J. Yuan, L. Zhang, *et al.*, "Three-dimensional location system based on an L-shaped array of Rydberg atomic receivers," Opt. Lett. **48**(15), 3945–3948 (2023).
4. A. Leal-Junior, C. Díaz, A. Frizera, *et al.*, "Highly sensitive fiber-optic intrinsic electromagnetic field sensing," Adv. Photonics Res. **2**(1), 2000078 (2021).
5. T. Bothwell, C. J. Kennedy, A. Aeppli, *et al.*, "Resolving the gravitational redshift across a millimetre-scale atomic sample," Nature **602**(7897), 420–424 (2022).
6. A. D. Cronin, J. Schmiedmayer, and D. E. Pritchard, "Optics and interferometry with atoms and molecules," Rev. Mod. Phys. **81**(3), 1051–1129 (2009).
7. G. Rosi, F. Sorrentino, L. Cacciapuoti, *et al.*, "Precision measurement of the Newtonian gravitational constant using cold atoms," Nature **510**(7506), 518–521 (2014).
8. J. A. Sedlacek, A. Schwettmann, H. Kübler, *et al.*, "Microwave electrometry with Rydberg atoms in a vapour cell using bright atomic resonances," Nat. Phys. **8**(11), 819–824 (2012).
9. J. C. Camparo, "Atomic stabilization of electromagnetic field strength using Rabi resonances," Phys. Rev. Lett. **80**(2), 222–225 (1998).
10. J. Yuan, H. Zhang, C. Wu, *et al.*, "Creation and control of vortex-beam arrays in atomic vapor," Laser Photonics Rev. **17**(5), 2200667 (2023).
11. S. L. S. Li, J. Yuan, and L. Wang, "Improvement of microwave electric field measurement sensitivity via multi-carrier modulation in Rydberg atoms," Appl. Sci. **10**(22), 8110 (2020).
12. Z. Zhang, S. Liang, I. Septembre, *et al.*, "Non-hermitian delocalization in a two-dimensional photonic quasicrystal," Phys. Rev. Lett. **132**(26), 263801 (2024).
13. Y. Han, D. Wu, K. Kasai, *et al.*, "Measurement of the wavefunction for a biphoton state with homodyne detection using least squares estimation," J. Opt. **22**(2), 025202 (2020).
14. J. Yuan, X. Wang, G. Chen, *et al.*, "High-fidelity frequency converter in high-dimensional spaces," Laser Photonics Rev. p. 2400368 (2024).
15. C. L. Holloway, M. T. Simons, J. A. Gordon, *et al.*, "Electric field metrology for SI traceability: Systematic measurement uncertainties in electromagnetically induced transparency in atomic vapor," J. Appl. Phys. **121**(23), 233106 (2017).

Optics EXPRESS

16. J. G. Coffer, B. Sickmiller, A. Presser, *et al.*, "Line shapes of atomic-candle-type Rabi resonances," Phys. Rev. A **66**(2), 023806 (2002).
17. T. F. Gallagher, *Rydberg Atoms, Cambridge Monographs on Atomic, Molecular and Chemical Physics* (Cambridge University Press, 1994).
18. C. L. Holloway, M. T. Simons, M. D. Kautz, *et al.*, "A quantum-based power standard: Using Rydberg atoms for a SI-traceable radio-frequency power measurement technique in rectangular waveguides," Appl. Phys. Lett. **113**(9), 094101 (2018).
19. C. G. Wade, N. Šibalic, N. R. de Melo, *et al.*, "Real-time near-field terahertz imaging with atomic optical fluorescence," Nat. Photonics **11**(1), 40–43 (2017).
20. Z. Song, H. Liu, X. Liu, *et al.*, "Rydberg-atom-based digital communication using a continuously tunable radio-frequency carrier," Opt. Express **27**(6), 8848 (2019).
21. B. Liu, L.-H. Zhang, Z.-K. Liu, *et al.*, "Highly sensitive measurement of a megahertz RF electric field with a Rydberg-atom sensor," Phys. Rev. Appl. **18**(1), 014045 (2022).
22. X. Y. I. Xu, G. Xie, J. Ma, *et al.*, "Fast simulation for interacting four-level Rydberg atoms: electromagnetically induced transparency and Autler-Townes splitting," Opt. Express **32**(12), 21755 (2024).
23. Y. Cai, S. Shi, Y. Zhou, *et al.*, "High-sensitivity Rydberg-atom-based phase-modulation receiver for frequency-division-multiplexing communication," Phys. Rev. Appl. **19**(4), 044079 (2023).
24. J. Yuan, W. Yang, M. Jing, *et al.*, "Quantum sensing of microwave electric fields based on Rydberg atoms," Rep. Prog. Phys. **86**(10), 106001 (2023).
25. M. Jing, Y. Hu, J. Ma, *et al.*, "Atomic superheterodyne receiver based on microwave-dressed Rydberg spectroscopy," Nat. Phys. **16**(9), 911–915 (2020).
26. J. A. Sedlacek, A. Schwettmann, H. Kübler, *et al.*, "Atom-based vector microwave electrometry using Rubidium Rydberg atoms in a vapor cell," Phys. Rev. Lett. **111**(6), 063001 (2013).
27. J. A. Gordon, M. T. Simons, A. H. Haddab, *et al.*, "Weak electric-field detection with sub-1 Hz resolution at radio frequencies using a Rydberg atom-based mixer," AIP Adv. **9**(4), 045030 (2019).
28. A. K. Robinson, N. Prajapati, D. Senic, *et al.*, "Determining the angle-of-arrival of a radio-frequency source with a Rydberg atom-based sensor," Appl. Phys. Lett. **118**(11), 114001 (2021).
29. F. Sun, J. Ma, Q. Bai, *et al.*, "Measuring microwave cavity response using atomic Rabi resonances," Appl. Phys. Lett. **111**(5), 051103 (2017).
30. X. Liu, Z. Jiang, J. Qu, *et al.*, "Microwave magnetic field detection based on Cs vapor cell in free space," Rev. Sci. Instrum. **89**(6), 063104 (2018).
31. C. Affolderbach, G.-X. Du, T. Bandi, *et al.*, "Imaging microwave and DC magnetic fields in a vapor-cell Rb atomic clock," IEEE Trans. Instrum. Meas. **64**(12), 3629–3637 (2015).
32. T. Swan-Wood, J. Coffer, and J. Camparo, "Precision measurements of absorption and refractive-index using an atomic candle," IEEE Trans. Instrum. Meas. **50**(5), 1229–1233 (2001).
33. E. Paradis, G. Raithel, and D. A. Anderson, "Atomic measurements of high-intensity VHF-band radio-frequency fields with a Rydberg vapor-cell detector," Phys. Rev. A **100**(1), 013420 (2019).
34. Y. Jiao, X. Han, Z. Yang, *et al.*, "Spectroscopy of Cesium Rydberg atoms in strong radio-frequency fields," Phys. Rev. A **94**(2), 023832 (2016).
35. J. Hu, H. Li, R. Song, *et al.*, "Continuously tunable radio frequency electrometry with Rydberg atoms," Appl. Phys. Lett. **121**(1), 014002 (2022).
36. L. Li, Y. Jiao, J. Hu, *et al.*, "Super low-frequency electric field measurement based on Rydberg atoms," Opt. Express **31**(18), 29228 (2023).
37. Y. Shi, C. Li, K. Ouyang, *et al.*, "Tunable frequency of a microwave mixed receiver based on Rydberg atoms under the Zeeman effect," Opt. Express **31**(22), 36255 (2023).
38. S. H. You, M. H. Cai, S. S. Zhang, *et al.*, "Microwave-field sensing via electromagnetically induced absorption of Rb irradiated by three-color infrared lasers," Opt. Express **30**(10), 16619 (2022).
39. X.-H. Liu, K.-Y. Liao, Z.-X. Zhang, *et al.*, "Continuous-frequency microwave heterodyne detection in an atomic vapor cell," Phys. Rev. Appl. **18**(5), 054003 (2022).
40. Y. Xue, Y. Jiao, L. Hao, *et al.*, "Microwave two-photon spectroscopy of Cesium Rydberg atoms," Opt. Express **29**(26), 43827–43835 (2021).
41. Z. Feng, X. Liu, Y. Zhang, *et al.*, "Atom-based sensing technique of microwave electric and magnetic fields via a single Rubidium vapor cell," Opt. Express **31**(2), 1692 (2023).
42. F. Sun, Z. Jiang, J. Qu, *et al.*, "Tunable microwave magnetic field detection based on Rabi resonance with a single Cesium-Rubidium hybrid vapor cell," Appl. Phys. Lett. **113**(16), 164101 (2018).
43. W. Yang, M. Jing, H. Zhang, *et al.*, "Radio frequency electric field-enhanced sensing based on the Rydberg atom-based superheterodyne receiver," Opt. Lett. **49**(11), 2938–2941 (2024).
44. N. Šibalic, J. Pritchard, C. Adams, *et al.*, "ARC: An open-source library for calculating properties of alkali Rydberg atoms," Comput. Phys. Commun. **220**, 319–331 (2017).
45. A. Tretiakov and L. J. LeBlanc, "Microwave Rabi resonances beyond the small-signal regime," Phys. Rev. A **99**(4), 043402 (2019).

Optics EXPRESS

46. A. K. Robinson, A. B. Artusio-Glimpse, M. T. Simons, *et al.*, "Atomic spectra in a six-level scheme for electromagnetically induced transparency and Autler-Townes splitting in Rydberg atoms," Phys. Rev. A **103**(2), 023704 (2021).
47. Z. Zhang and S. Satpathy, "Electromagnetic wave propagation in periodic structures: Bloch wave solution of Maxwell's equations," Phys. Rev. Lett. **65**(21), 2650–2653 (1990).